Cite this article
Katayama N, Lin C, Inadomi S *et al.* (2026)
Bridge assessment after 2024 Noto Peninsula earthquake and rainfall using point cloud.
Proceedings of the Institution of Civil Engineers – Forensic Engineering **179(2)**: 49–58,
https://doi.org/10.1680/jfoen.25.00024

Research Article
Paper 2500024
Received 15/05/2025; Accepted 08/09/2025

Forensic Engineering

emerald PUBLISHING ice Publishing

Bridge assessment after 2024 Noto Peninsula earthquake and rainfall using point cloud

Naomichi Katayama
Daiichi-Consultants Co. Ltd., Kochi, Japan (Orcid:0009-0007-9438-1893)

Chao Lin
Department of Civil Engineering, The University of Tokyo, Tokyo, Japan
(Orcid:0000-0002-1517-8392)

Shogo Inadomi
Department of Civil Engineering, The University of Tokyo, Tokyo, Japan
(Orcid:0009-0009-3742-0299)

Kenta Itakura
ImVisionLabs Inc., Tokyo, Japan (Orcid:0000-0001-7259-271X)

Yu Chen
Department of Civil Engineering, The University of Tokyo, Tokyo, Japan
(Orcid:0000-0002-1187-4761)

Pang-Jo Chun
Department of Civil Engineering, The University of Tokyo, Tokyo, Japan
(Orcid:0000-0002-9755-8435) (corresponding author: chun@g.ecc.u-tokyo.ac.jp)

This study addresses the challenge of assessing bridge damage progression under compound disasters, specifically focusing on Bridge A in Japan affected by the 2024 Noto Peninsula Earthquake and subsequent heavy rainfall. We aimed to quantitatively evaluate potential changes in pier inclination using multi-temporal point cloud data (PCD) acquired by way of terrestrial LiDAR immediately after the earthquake and following the rainfall. Accurate pier isolation from complex PCD, complicated by environmental changes such as sediment deposition, was achieved using a deep learning semantic segmentation model enhanced with low-rank adaptation fine-tuning. Two distinct geometric analysis methods, M-estimator sample consensus (MSAC) cylinder fitting and principal component analysis (PCA) based on local surface normals, were independently applied to the segmented pier data to calculate inclination angles. Both MSAC and PCA consistently revealed a slight pier inclination ranging from 1.7° to 3° after the earthquake but detected no statistically significant progression after the heavy rainfall event. Our findings indicate no measurable progression of pier inclination during the observation period, demonstrating the effectiveness of the proposed workflow combining advanced scanning, segmentation, and robust multiple geometric analysis methods for monitoring structural stability and resilience in multi-hazard scenarios.

Keywords: bridges/deformation/durability/earthquakes/health and safety/maintenance and inspection

Notation

$\overrightarrow{n_1} = (x_1, y_1, z_1)$	the normal of the bridge pier before the rainfall
$\overrightarrow{n_2} = (x_2, y_2, z_2)$	the normal of the bridge pier after the rainfall
$\overrightarrow{n_g} = (0, 0, 1)$	the normal vector of the ground
θ	rotation angle of the pier caused by the rainfall
θ_1	inclination angle of the pier before the rainfall
θ_2	inclination angle of the pier after the rainfall

1. Introduction

The Noto Peninsula Earthquake, which struck in January 2024, inflicted severe damage across a wide area in Japan, primarily in the Noto region of Ishikawa Prefecture, affecting infrastructure, including roads and bridges. This event starkly underscored the vulnerability of infrastructure to seismic disasters and the critical need for prompt and precise response measures. In the immediate aftermath of an earthquake, rapid road clearance is essential for rescue operations, logistics, and the recovery of the regional economy. Achieving this requires swiftly assessing bridge damage, determining the need for traffic restrictions based on load-bearing capacity and trafficability, and implementing emergency countermeasures when necessary.

Current post-earthquake emergency inspection practices in Japan, typically guided by established manuals, face several inherent challenges. These include limited personnel, the absence of standardised quantitative criteria, and a heavy reliance on the subjective judgement of engineers, who themselves may be physically and psychologically stressed due to the disaster. The 2024 Noto Peninsula Earthquake further compounded these issues, as it was followed by sequential heavy rainfall and flooding events. This combination of disasters raised concerns that structures potentially weakened by the initial seismic event might be vulnerable to additional damage or accelerated deterioration from the subsequent hazards. Consequently, establishing methodologies for continuously monitoring and evaluating changes in structural integrity under such compound disaster conditions has become an urgent priority.

To address these challenges, recent research has increasingly focused on leveraging point cloud data (PCD) acquired by three-dimensional (3D) laser scanners for bridge maintenance and disaster response (Chen *et al*., 2025; Truong-Hong and Lindenbergh, 2022). PCD is capable of detailed, non-contact, 3D measurement of structural geometry and is effective for identifying damage locations and quantitatively assessing displacements and deformations. In our previous work (Katayama and Chun, 2025), we conducted emergency inspections and acquired PCD for a group of damaged bridges, including Bridge A in the Noto region, immediately after the 2024 Noto Peninsula Earthquake. This investigation highlighted the potential of PCD for detailed damage documentation and information sharing, facilitating remote expert participation in the diagnostic process. Specifically, for Bridge A, preliminary analysis of the PCD indicated a pier inclination of approximately 1.0°. However, data from a single time point posed difficulty in ascertaining whether this inclination was pre-existing, newly induced by the earthquake, or potentially progressive due to aftershocks or other factors. This limitation emphasised the critical importance of temporal monitoring for accurately evaluating post-disaster structural integrity. Compared with traditional methods such as inclinometers, which measure tilt at discrete points, PCD provides a comprehensive 3D representation of the entire structure. This enables not only the analysis of inclination but also the detection of more complex deformation modes and interaction with surrounding geological features, offering a more holistic approach to structural health monitoring.

In the context of a compound disaster—an earthquake followed by severe rainfall and flooding—this study aims to evaluate how a bridge potentially compromised by the seismic event responds to subsequent natural hazards, specifically through an assessment of the temporal evolution of its structural health. The analytical workflow involves two main steps. First, we employ deep learning (DL)-based PCD semantic segmentation (SS) techniques, specifically refined for this study, to accurately extract the target pier components from the complex bridge geometry. Second, we apply geometric analysis methods designed to ensure reproducibility and objectivity—namely, M-estimator sample consensus (MSAC) (Torr and Zisserman, 2000) and principal component analysis (PCA) (Pearson, 1901)—to the extracted pier PCD. This enables the high-precision quantitative calculation of pier inclination angles at both time points (post-earthquake and post-rainfall), thereby eliminating user-dependent variability. By quantitatively comparing these angles, we evaluate the impact of the secondary event (heavy rainfall and flooding) on the pier inclination, which may have been affected by the initial earthquake. This study presents a quantitative methodology using time-series PCD to assess structural changes under compound disasters. Our approach offers valuable insights for post-disaster bridge monitoring, risk assessment, and the advancement of structural health monitoring and disaster response planning.

2. Methodology

The overall workflow comprises three primary steps: (*i*) acquisition of PCD for the target bridge at two distinct time points—immediately after the earthquake and after the heavy rainfall; (*ii*) extraction of pier components from the complex bridge PCD using a DL-based SS model enhanced by way of fine-tuning; and (*iii*) application of geometric analysis techniques, specifically MSAC and PCA, to the segmented pier PCD to precisely calculate the pier inclination angle at each time point and evaluate the change between them. Each step is detailed further in the following subsections.

2.1 Data preparation

To enable comparative analysis of the structural geometry of Bridge A over time, two distinct PCD files were acquired. The first data were collected shortly after the 2024 Noto Peninsula Earthquake (referred to as the 'post-earthquake' PCD), and the second one was acquired after the heavy rainfall event in September 2024 (the 'post-rainfall' PCD).

Both datasets were collected on-site using the Matterport Pro3, a professional-grade 3D camera equipped with light detection and ranging (LiDAR) technology. The technical specifications of the device relevant to this study are summarised in Table 1. It offers an accuracy of ±20 mm at a distance of 10 m. When combined with repeated measurements and data integration, this level of precision readily supports reliable estimation of pier inclination and other subtle geometric changes in bridge structures. During the on-site data acquisition campaigns, multiple scans were captured from various positions around and beneath the bridge to minimise occlusions and ensure comprehensive coverage of the pier and other relevant structural elements, consistent with the procedure described in our previous work. Figure 1 shows photographs of the target bridge. In Figure 1(a), the Matterport device was set up on the riverbed, and in Figure 1(b), it was placed on the abutment side. The red boxes indicate the locations of the Matterport device used for PCD measurement.

2.2 SS model for pier isolation

Accurate isolation of the bridge pier components from the raw PCD is a prerequisite for the subsequent geometric analysis of inclination. While the pier is the primary component of interest, the segmentation model is designed to classify all major bridge elements, including the superstructure, such as girders and deck, as well as the substructure. This approach serves two purposes. First, by training the model to learn the distinct features of various components, it improves boundary identification and enables a more precise extraction of the pier. Second, demonstrating the model's capability to segment the entire structure validates its capacity to capture bridge topology, which in turn supports the reliability of the pier segmentation. This study employed a DL-based SS approach to automatically and reliably classify each

Table 1. Technical specifications for scanning of the Matterport Pro3

Accuracy	Operating range	Acquisition rate	Depth resolution	Field of view
±20 mm at 10 m	0.5–100 m	10^5 points per second	1.5×10^5 points per scan	360° Horizontal/295° Vertical

Figure 1. Photographs of the target bridge. The red boxes indicate the locations of the Matterport device used for PCD measurement

point in the PCD into predefined categories, thereby isolating the points belonging to the bridge pier.

The core framework utilised in this study is a PointNet++-based model (Qi *et al*., 2017) that incorporates bridge-specific spatial information, which enhances feature learning through the integration of location- and structure-oriented information pertinent to bridge components (Lin *et al*., 2025). This approach improves segmentation performance through specialised feature extraction mechanisms and position-aware loss functions tailored for bridge structural elements. The method leverages contextual information, such as the relative spatial relationships between different bridge parts; for example, piers typically support girders. It also recognises inherent geometric characteristics of components, such as the columnar shape of piers. These techniques together lead to more robust and accurate segmentation compared with generic PCD SS models. The model was trained on a large-scale, publicly available dataset curated by Lu *et al*. (2019). This dataset comprises diverse PCD scans of bridges, including numerous examples of pier structures under different conditions. Training on this dataset enables the model to learn generalisable features representative of common bridge components, enhancing its adaptability to new, unseen bridge data.

To address the environmental variability and enhance the model's robustness to the altered site conditions, we implemented a targeted fine-tuning strategy using low-rank adaptation (LoRA) (Hu *et al*., 2022). LoRA is a parameter-efficient fine-tuning technique that adapts large pre-trained models to specific downstream tasks or datasets. Instead of re-training all model parameters, LoRA introduces trainable low-rank matrices into specific layers while keeping the original pre-trained weights frozen. It is commonly applied to attention layers in transformer-based models. In this study, LoRA fine-tuning was specifically applied to improve the classification accuracy of the highly variable background class, which now includes sediment deposits. The model was adapted to better distinguish the flood-altered surroundings from the structural elements, particularly the bases of bridge piers. The aim is to significantly improve the precision of pier segmentation despite the challenging post-flood environmental conditions.

2.3 Inclination and rotation angle calculation

The inclination and rotation angles were acquired through two steps. First, the normals of the same bridge pier before and after the rainfall, denoted as $\overrightarrow{n_1} = (x_1, y_1, z_1)$ and $\overrightarrow{n_2} = (x_2, y_2, z_2)$, were calculated using the extracted PCD. Second, the inclination angles of the pier before and after the rainfall (i.e. θ_1 and θ_2) were obtained using the dot product between each normal vector and the ground surface normal vector $\overrightarrow{n_g} = (0, 0, 1)$. The rotation angle of the pier caused by the rainfall θ was computed using the dot product between $\overrightarrow{n_1}$ and $\overrightarrow{n_2}$. The dot product formula is

$$1.\quad \cos\theta = \frac{x_1x_2 + y_1y_2 + z_1z_2}{\sqrt{x_1^2 + y_1^2 + z_1^2} \times \sqrt{x_2^2 + y_2^2 + z_2^2}}$$

In this study, $\overrightarrow{n_1}$ and $\overrightarrow{n_2}$ were estimated using two different methods, MSAC and PCA, resulting in two sets of vectors: one obtained entirely with MSAC and the other entirely with PCA.

2.3.1 Pier axis estimation using MSAC

To quantify the inclination of the pier from the segmented PCD, estimating its central axis direction vector is essential. We employed MSAC (Torr and Zisserman, 2000), a robust model fitting algorithm derived from random sample consensus (RANSAC) (Fischler and Bolles, 1981), known for its enhanced stability against outliers commonly found in real-world data. Unlike standard RANSAC, MSAC uses M-estimators to assign continuous penalty scores based on point-to-model distances, often yielding more accurate results when the proportion of outliers is high or the distinction between inliers and outliers is ambiguous.

MSAC iteratively fits candidate models (e.g. cylinders for piers) to random minimal subsets of the data and selects the model minimising a robust cost function summed over all points. This robustness is crucial for PCD of bridge piers, which ideally represents regular shapes such as cylinders but often contains noise, occlusions, segmentation errors, and surface irregularities that act as outliers. MSAC can reliably estimate the underlying geometry of the pier, specifically its axis direction, even from such imperfect data.

2.3.2 Pier axis estimation using PCA

PCA is a fundamental statistical technique widely used for dimensionality reduction and feature extraction in multivariate datasets (Pearson, 1901). It works by identifying orthogonal directions, known as principal components, along which the variance of the data is maximised. The standard procedure involves: (*i*) mean-centring the data, (*ii*) computing the covariance matrix of the centred data, and (*iii*) performing an eigenvalue decomposition of the covariance matrix to obtain the eigenvalues and corresponding eigenvectors. The eigenvectors represent the directions of the principal components, and the eigenvalues indicate the variance of the data along those directions.

To estimate the axis of a bridge pier, PCA was applied under the assumption that the pier has a uniform cross-section, such as a cylinder or prism. We leveraged the geometric property that the normal vectors of points on the lateral surface of the pier are ideally perpendicular to its central axis. Therefore, instead of directly applying PCA to the point coordinates, we first estimated the local surface normal vector for each point within the segmented pier PCD. These normal vectors were expected to lie predominantly within or close to a plane perpendicular to the pier axis. Accordingly, the direction along which these normal vectors exhibit the least variance should correspond to the direction of the pier axis. In the context of PCA, this direction is given by the eigenvector associated with the smallest eigenvalue. This direction, which is equivalently the most orthogonal direction to the set of normal vectors, is regarded as the principal axis direction of the pier.

The local surface normal vector at each point was estimated using a standard local neighbourhood-based technique. For each point p, its k nearest neighbours within the pier PCD were identified. A local tangent plane was then fitted to this neighbourhood by applying PCA to the coordinates of the neighbouring points. The eigenvector corresponding to the smallest eigenvalue was taken as the normal of the plane and assigned as the estimated normal vector for point p. Based on preliminary analysis and standard practice for cylindrical shapes, the number of neighbours k was set to 60 in this study. For the selection of this setting, we analysed the local point cloud density in the Matterport-derived bridge pier data. For each point, we computed the distances to its 60 nearest neighbours. The average distance to these neighbours was 0.016 m, while the median was 0.015 m. These values indicate that $k = 60$ corresponds to a physical scale of approximately 1.5 cm, which is small relative to the curvature of the bridge pier surface. This scale is therefore appropriate for assuming local planarity while still being large enough to reduce the effect of measurement noise.

3. Experimental results

Bridge A is a reinforced concrete bridge with a length of 24.0 m and a width of 5.5 m, located on the Noto Peninsula, Japan. Based on our previous survey conducted immediately after the 2024 Noto Peninsula Earthquake, this bridge was identified as having a potentially inclined pier, making it a pertinent case for monitoring post-disaster geometric changes. Regarding the pier inclination, we did not conduct an independent field measurement using a total station or inclinometer.

3.1 Dataset and ground truth preparation

As detailed in Section 2.1, the primary dataset for this study consists of two PCD files of Bridge A, captured using the Matterport Pro3. To quantitatively evaluate the performance of the proposed SS model (detailed in Section 2.2), ground truth labels for both PCD files were manually annotated on a point-by-point basis. Each point in the datasets was assigned to one of five predefined semantic categories: pier, girder, deck, parapet, and others (background). These manually annotated datasets serve as the ground truth for assessing the accuracy of the SS model in Section 3.2, enabling the calculation of standard evaluation metrics such as intersection over union, accuracy, and F1-score for each semantic class.

3.2 PCD SS

Figure 2 presents the SS results of the bridge PCD using the refined SS network. The visualisation demonstrates the model's ability to accurately identify and segment various bridge components. The pier, shown in green, is distinctly recognised under both environmental conditions. Despite the significant terrain changes following the earthquake and rainfall events, the model maintains consistent segmentation performance, particularly for the pier structure. The colour-coded classification results reveal that while some minor misclassifications occur between background and structural elements in the post-rainfall scenario, the core structural components maintain reliable segmentation integrity.

The quantitative performance metrics in Table 2 confirm the robustness of the refined SS model for pier identification across different environmental conditions. The classification metrics for the pier remain substantially higher than those for other structural components. This demonstrates that despite not being specifically trained on the current dataset, the model effectively transfers knowledge from the training dataset to accurately identify the pier even under significantly altered environmental conditions.

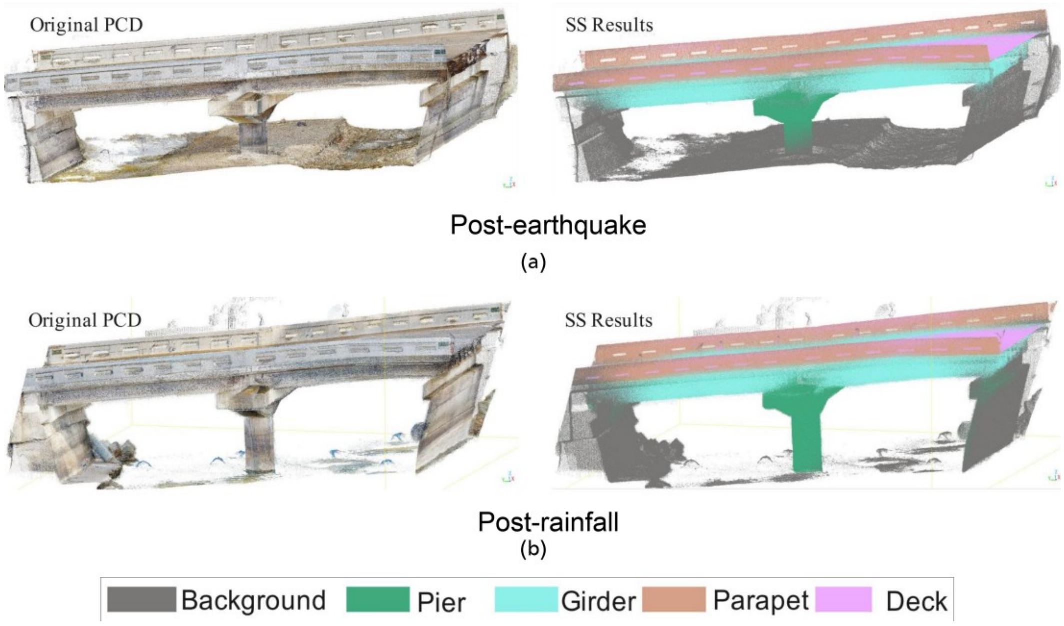

Figure 2. SS results of PCD

Table 2. Quantitative analysis of PCD SS results (%)

	IoU						Accuracy						
	Backg.	Pier	Girder	Deck	Parapet	Mean	Backg.	Pier	Girder	Deck	Parapet	Mean	**F1 score**
Post-earthquake	81.0	88.6	57.7	57.0	59.1	68.7	96.1	98.4	87.0	61.7	62.5	81.1	82.2
Post-rainfall	76.5	82.9	63.6	65.3	67.1	71.1	98.9	86.6	88.4	68.5	72.3	82.9	84.0

Figure 3 presents the confusion matrices, offering a detailed quantitative breakdown of the SS model's performance for both the post-earthquake and post-rainfall datasets. The key observation is the high concentration of values along the main diagonal, which represents correctly classified points (true positives). For instance, in both scenarios, the number of points correctly identified as 'Pier', 2 199 702 in the post-earthquake case and 2 508 498 in the post-rainfall case, is significantly higher than that of any misclassifications in the corresponding rows or columns.

A closer look at the off-diagonal elements reveals that the primary confusions for the 'Pier' class occur with the 'Background' and 'Girder' classes. This is geometrically intuitive, as these components are physically adjacent to the pier. However, the crucial takeaway is that the number of true positives for the pier class substantially exceeds these misclassifications. This demonstrates the model's robustness in distinguishing the core pier structure from its surroundings, even under significant environmental changes such as sediment deposition. It validates the effectiveness of the LoRA fine-tuning in adapting the model to the altered background.

Figure 4 isolates and visualises the classification results specifically for the 'Pier' class, providing a clear measure of its identification accuracy. Two key observations emerge from these charts.

First, the model achieves exceptionally high accuracy for the target class in both datasets. Post-earthquake, 86.6% of the true pier points were correctly classified, and this rate even further increased to 98.4% post-rainfall. This demonstrates the model's strong generalisation capability and its effectiveness despite the challenging real-world conditions.

Second, the proportion of misclassifications was small, and their nature was interpretable. Most errors involved misidentification between the pier and either 'Background' or 'Girder'. For instance, 10.5% of pier points were classified as 'Background' in the post-earthquake case. Importantly, misclassifications into geometrically dissimilar and distant classes such as 'Deck' and 'Parapet' were negligible, at 0.0%. This high level of accuracy, combined with the predictable nature of the minor errors, demonstrates that the segmented pier point clouds are of sufficient quality and reliability for the subsequent high-precision geometric analysis of inclination.

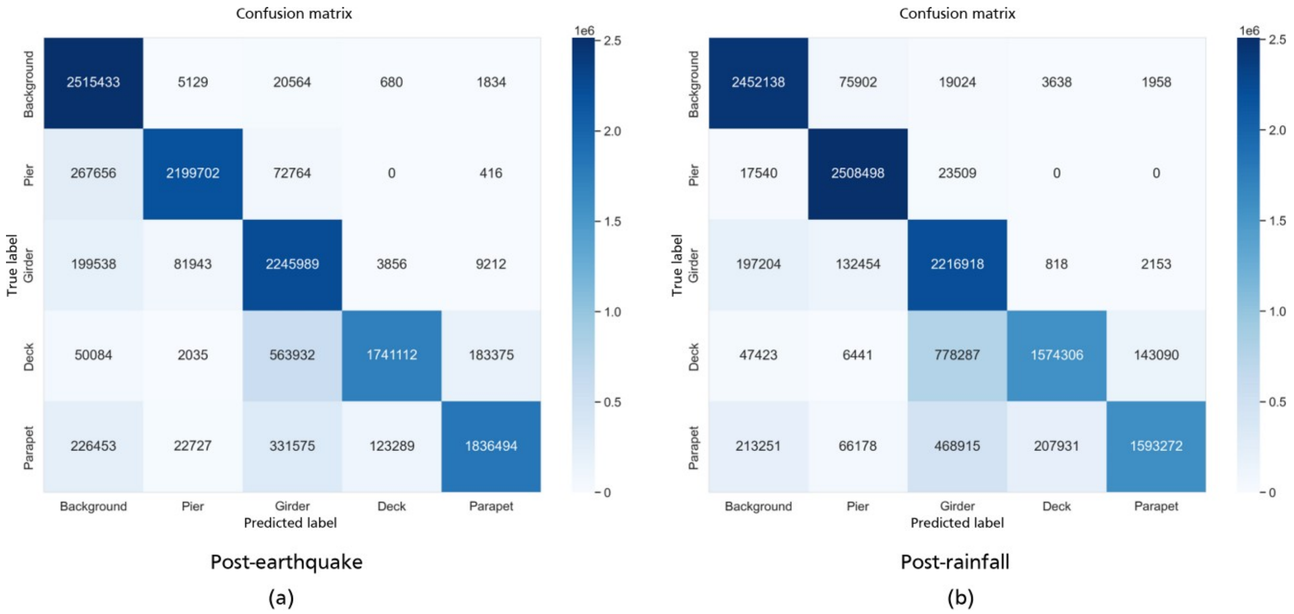

Figure 3. Confusion matrix of SS results

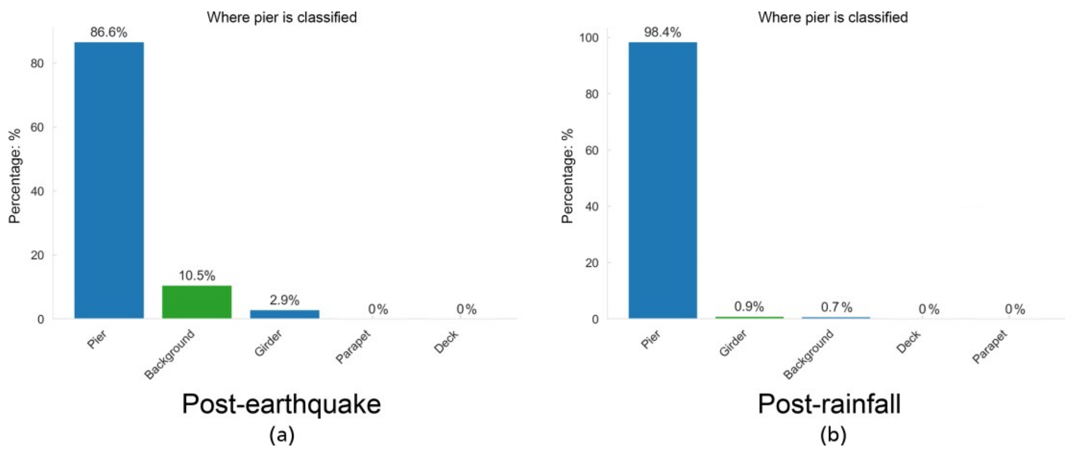

Figure 4. Target (Pier) class confusion results

3.3 Inclination and rotation angle calculation

3.3.1 Results using MSAC

The MSAC algorithm was employed to fit a cylinder model to both post-earthquake and post-rainfall pier PCD. A cylinder is defined as

2. $$(x-x_0)^2+(y-y_0)^2+(z-z_0)^2-\left(\frac{(x-x_0)a+(y-y_0)b+(z-z_0)c}{\sqrt{a^2+b^2+c^2}}\right)^2=r^2$$

The fitting results are illustrated in Figure 5, which shows the original PCD and the fitted cylinder in orange. These results confirm that the MSAC algorithm appropriately captured the cylindrical geometry of the target pier.

Recognising that MSAC incorporates random sampling and can thus yield slightly different results across runs, we performed 1000 independent repetitions of the MSAC cylinder fitting process to ensure the reliability of the estimated axis vectors. The analysis of the repeated computations revealed that the estimated inclination angles for both the post-earthquake (θ_1) and post-rainfall (θ_2) states consistently fell within a range of approximately 2° to 3° from the vertical, as shown in Figure 6. As summarised in Table 3, the mean inclination angles showed no significant difference between the two time points. Consequently, the analysis utilising robust repeated MSAC fitting

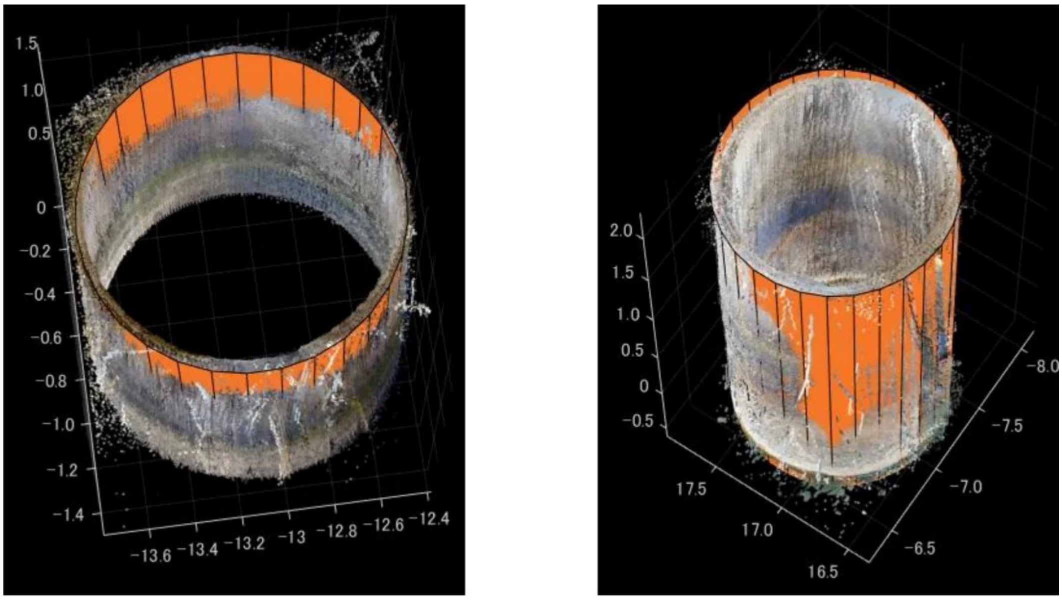

Figure 5. Visualisation of MSAC calculation

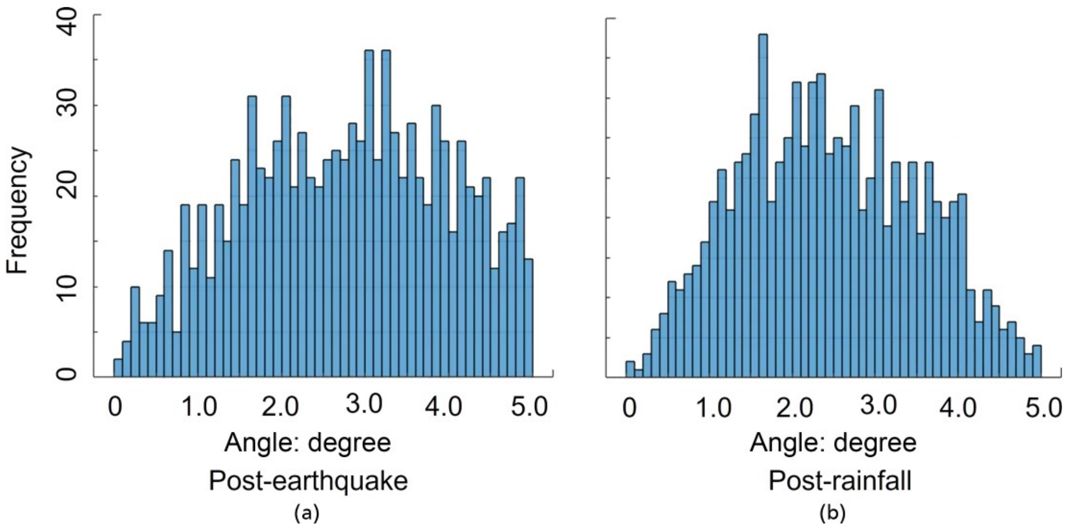

Figure 6. Results of 1000 independent repetitions of the MSAC cylinder fitting process

Table 3. Results by MSAC

Inclination angle after earthquake	Inclination angle after rainfall
2.76°	2.45°

detected no discernible change, in particular, no significant increase in inclination attributable to the heavy rainfall event.

3.3.2 Results using PCA

To enhance the robustness of the estimation against potential local variations or noise in the PCD, the final axis vector used for angle calculation was determined by averaging the axis vectors obtained from applying the PCA analysis to 60 randomly sampled subsets of the pier's lateral surface points. While PCA applied to the full dataset is deterministic, this averaging over subsets was aimed to provide a more stable representation of the overall pier orientation.

The PCA results are illustrated in Figure 7, and Table 4 presents the inclination angles calculated by the PCA method. The results show that the pier exhibited a slight inclination of approximately 1.7° from the vertical under both conditions. Specifically, the inclination angle was calculated to be 1.70° for the post-earthquake state (θ_1) and 1.67° for the post-rainfall state (θ_2).

Notably, the difference between the inclination angles before and after the rainfall event was minimal. This indicates that the PCA method, even with the averaging step, did not detect any significant change in the pier, consistent with the findings from the MSAC analysis. At the same time, this result further supports the stability and robustness of the PCA method.

3.4 Discussion

The convergence of findings from these two fundamentally different approaches—one relying on fitting a global geometric model (MSAC) and the other on analysing the distribution of local geometric features (PCA)—significantly strengthens confidence in the primary conclusion. Specifically, the heavy rainfall event did not cause a detectable progression in the inclination of the Bridge A pier within the scope of the acquired data and the applied analysis techniques. The slight difference in the absolute inclination values reported by the two methods, approximately 2–3° for MSAC compared with 1.7° for PCA, is likely to be attributed to their inherent methodological differences. MSAC fits an idealised overall shape, while PCA is more influenced by the precise distribution and orientation of points on the pier surface. However, both methods concur that the change in inclination over the period was negligible.

Table 4. Results by PCA

Inclination angle after earthquake	Inclination angle after rainfall
1.70°	1.67°

This outcome suggests that, although the pier exhibited some inclination after the initial earthquake, its condition remained relatively stable throughout the subsequent period, including the heavy rainfall. This implies that the foundation and surrounding soil conditions, despite the seismic impact and subsequent rainfall, were sufficient to prevent further significant tilting during this timeframe. It also highlights the value of multi-temporal point cloud monitoring for both detecting local damage progression and confirming structural stability, which is crucial for informed decision making regarding infrastructure safety and usability after disasters.

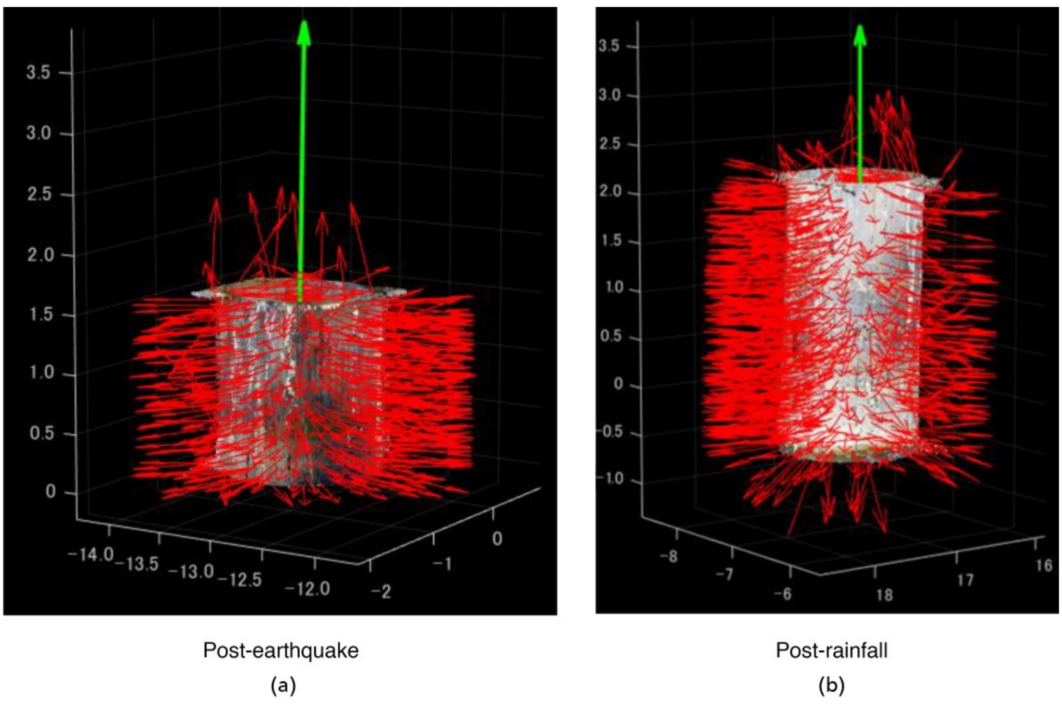

Figure 7. Visualisation of PCA calculation

MSAC applies cylinder fitting—a global parametric model—to the entire pier surface; therefore, departures from an ideal cylinder can bias the fitted axis. In contrast, PCA computes and aggregates local surface normal features within fixed neighbourhoods and is therefore influenced primarily by the lateral surface. This difference between global cylinder fitting and local feature aggregation explains the discrepancy in the inclination values, although both methods consistently show no progression between the two epochs.

While the consistency between MSAC and PCA enhances the reliability of the findings, certain limitations should still be acknowledged. The accuracy in detecting small changes is inherently tied to the quality of the input PCD captured by the scanner, including its density, noise level, and measurement accuracy. Furthermore, the results might be influenced to some extent by the specific parameters chosen for each algorithm, such as the inlier threshold for MSAC, the neighbourhood size k, and the averaging strategy for PCA. Because no independent ground truth survey was obtained, we cannot determine which method is more accurate for this dataset. Both MSAC and PCA yield consistent trends and indicate no progression between the post-earthquake and post-rainfall epochs. In future work, we will collect ground truth measurements with instruments such as a total station and an inclinometer and systematically compare global cylinder fitting with local normal aggregation. While this study presents a valuable snapshot, continuous, long-term monitoring using consistent methods would be ideal for definitively tracking structural behaviour. In addition, the acquired PCD includes the geometry of the riverbed and abutments. Although not analysed in this study, this contextual data holds significant potential for future research, particularly for assessing scour progression and slope stability, as well as for correlating these environmental changes with the structural response of the bridge. Moreover, determining whether the inclination of approximately 1.7–3° captured in the initial measurement was solely caused by the earthquake or partially pre-existing would require baseline data before the seismic event.

Future research could involve sensitivity analyses on the impact of data quality and algorithm parameters, comparison with other axis estimation techniques, and integration of data from other sensors, such as geotechnical sensors, for a more holistic assessment. Applying this combined segmentation and multi-method geometric analysis workflow to a broader range of bridges and structural elements affected by various hazard sequences would provide further evidence of its robustness and utility.

4. Conclusion

This study aimed to quantitatively assess potential changes in pier inclination of Bridge A, affected by the 2024 Noto Peninsula Earthquake and subsequent heavy rainfall, using multi-temporal PCD. Post-earthquake and post-rainfall PCD were analysed through a DL-based SS model fine-tuned with LoRA for accurate pier extraction, followed by geometric analysis using MSAC and PCA. Both geometric analysis methods independently detected an initial inclination of approximately 1.7–3° but found no statistically significant change after rainfall, indicating geometric stability during the observation period. By increasing the number of independent samples, multiple inclination estimates can be generated for each epoch, allowing statistical hypothesis testing (e.g. Welch's t test) to examine whether differences before and after flooding are significant.

Key contributions of this research include: (*i*) establishing a workflow that combines LiDAR scanning, advanced PCD SS, and geometric analysis for monitoring structural response to compound disasters; (*ii*) demonstrating the robustness of the refined SS model under post-disaster conditions; (*iii*) validating the importance of using multiple analysis methods for reliable interpretation; and (*iv*) highlighting the role of systematic data collection in understanding infrastructure performance under multi-hazard scenarios.

Acknowledged limitations include the potential dependence of results on PCD quality and algorithm parameters and the absence of pre-earthquake baseline data to ascertain the origin of the initial inclination. Future research directions should involve sensitivity analyses, long-term monitoring, comparison with other estimation techniques, potentially incorporating higher-precision surveying methods, and extending the application of this workflow to other structures and disaster contexts to further validate its capabilities in infrastructure resilience assessment.

Funding

This work was partially supported by the Council for Science, Technology and Innovation (CSTI), the Cross-Ministerial Strategic Innovation Promotion Programme (SIP), the 3rd period of SIP 'Smart Infrastructure Management System' (Grant No. JPJ012187) (Funding agency: Public Works Research Institute) and the JSPS Grant-in-Aid for Scientific Research (Grant Nos. 21H01417, 22H01561, and 23H00198), and the China Scholarship Council (Grant No. 202306210048).

REFERENCES

Chen Y, Lin C, Kubo S *et al.* (2025) Automated dimension estimation of bridge components using semantic segmentation and geometric fitting of point cloud data. *Engineering Structures* **342**: 120837, 10.1016/j.engstruct.2025.120837.

Fischler MA and Bolles RC (1981) Random sample consensus: a paradigm for model fitting with applications to image analysis and automated cartography. *Communications of the ACM* **24(6)**: 381–395, 10.1016/b978-0-08-051581-6.50070-2.

Hu EJ, Shen Y, Wallis P *et al.* (2022) Lora: low-rank adaptation of large language models. *ICLR* **1(2)**: 3, 10.48550/arXiv.2106.09685.

Katayama N and Chun P (2025) *3D Model Data of Digital Twin in Seismic Emergency Inspection of Road Bridges. Tokyo*, Japan.

Lin C, Abe S, Zheng S *et al.* (2025) A structure-oriented loss function for automated semantic segmentation of bridge point clouds. *Computer-Aided Civil and Infrastructure Engineering* **40(6)**: 801–816, 10.1111/mice.13422.

Lu R, Brilakis I and Middleton CR (2019) Detection of structural components in point clouds of existing RC bridges. *Computer-Aided Civil and Infrastructure Engineering* **34(3)**: 191–212, 10.1111/mice.12407.

Pearson K (1901) LIII. On lines and planes of closest fit to systems of points in space. *The London, Edinburgh, and Dublin Philosophical Magazine and Journal of Science* **2(11)**: 559–572, 10.1080/14786440109462720.

Qi CR, Yi L, Su H *et al.* (2017) Pointnet++: deep hierarchical feature learning on point sets in a metric space. *Advances in Neural Information Processing Systems: 30*, 10.48550/arXiv.1706.02413.

Torr PH and Zisserman A (2000) MLESAC: a new robust estimator with application to estimating image geometry. *Computer Vision and Image Understanding* **78(1)**: 138–156, 10.1006/cviu.1999.0832.

Truong-Hong L and Lindenbergh R (2022) Automatically extracting surfaces of reinforced concrete bridges from terrestrial laser scanning point clouds. *Automation in Construction* **135**: 104127, 10.1016/j.autcon.2021.104127.

How can you contribute?

To discuss this paper, please email up to 500 words to the editor at support@emerald.com. Your contribution will be forwarded to the author(s) for a reply and, if considered appropriate by the editorial board, it will be published as discussion in a future issue of the journal.

Proceedings journals rely entirely on contributions from the civil engineering profession (and allied disciplines). Information about how to submit your paper online is available at www.emeraldgrouppublishing.com/journal/jfoen, where you will also find detailed author guidelines.